Available online at www.sciencedirect.com
ScienceDirect
Geochimica et Cosmochimica Acta 73 (2009) 5483–5492
Geochimica et Cosmochimica Acta
www.elsevier.com/locate/gca

In situ identification of a CAI candidate in 81P/Wild 2 cometary dust by confocal high resolution synchrotron X-ray fluorescence

Sylvia Schmitz [a,*], Frank E. Brenker [a], Tom Schoonjans [b], Bart Vekemans [b], Geert Silversmit [b], Laszlo Vincze [b], Manfred Burghammer [c], Christian Riekel [c]

[a] Geosciences Institute/Mineralogy, Goethe University Frankfurt, Altenhoeferallee 1, D-60438 Frankfurt, Germany
[b] Department of Analytical Chemistry, Ghent University, Krijgslaan 281 S12, B-9000 Ghent, Belgium
[c] ESRF, 6 rue Jules Horowitz, BP220, F-38043 Grenoble Cedex, France

Received 17 December 2008; accepted in revised form 9 June 2009; available online 16 June 2009

Abstract

We detected additional CAI-like material in STARDUST mission samples of comet 81P/Wild 2. Two highly refractory cometary dust fragments were identified in the impact track 110 [C2012, 0, 110, 0, 0] by applying high resolution synchrotron induced confocal and conventional XRF analysis (HR SR-XRF). The use of a polycapillary lens in front of the detector for confocal spectroscopy dramatically improves the fidelity of particle measurements by removing contribution from the surrounding aerogel. The high spatial resolution (300×300 nm^2; 300×1000 nm^2) obtained allowed the detailed non-destructive in situ (trapped in aerogel) study of impacted grains at the sub-μm level.

For the two largest particles of the track, the terminal particle and a second particle along the impact track, Ca concentration is up to 30 times higher than CI and Ti is enriched by a factor of 2 compared to CI. High resolution (HR) SR-XRF mapping also reveals that the highest concentrations of Ca, Ti, Fe (and Ni) measured within each grain belongs to different areas of the respective maps which indicate that the particles are composed of several chemically diverse mineral phases. This is in agreement with the finding of a complex phase assemblage of highly refractory minerals in the first ever detected Stardust mission CAI grain "Inti" of Track 25.

Principle component analysis (PCA) is a powerful tool for extracting the dominant mineral components and was applied to the two grains indicating that regions in the terminal particle and the second particle are consistent with anorthite or grossite and gehlenite, monticellite or Dmitryivanovite ($CaAl_2O_4$), respectively.

Our new findings demonstrate that the HR SR-XRF with confocal geometry and PCA analysis is capable of identifying CAI-like fragments without the need to extract particles from the aerogel matrix which is a time-consuming, complex and destructive process.

Furthermore, the detection of new CAI-like fragments in the coma dust of comet 81P/Wild 2 strengthens the observation that strong mixing effects and, therefore, mass transport before or during comet formation must have occurred at least up to the region where Kuiper Belt comets formed (~30 AU).

1. INTRODUCTION

Comet 81P/Wild 2 is a Jupiter family comet (JFC) which was gravitationally forced into its current orbit in 1974 by a close encounter with Jupiter and is believed to have originated in the Kuiper Belt. Comets were made up of relict material from the solar nebula and are believed to have not been (strongly) changed since, e.g., by thermal metamorphism or hydrous alteration. As a remnant from the Kuiper Belt, Wild 2 is supposed to be composed of submicron- to micron-sized silicates, sulphides, oxides, carbides,

* Corresponding author.
E-mail address: schmitz@em.uni-frankfurt.de (S. Schmitz).

0016-7037/$ - see front matter © 2009 Elsevier Ltd. All rights reserved.
doi:10.1016/j.gca.2009.06.008

phosphates and organic matter of solar and presolar origin (Sandford et al., 2006; Zolensky et al., 2006; Rotundi et al., 2008); most grains are expected to have escaped extensive thermal processing in the solar nebula. Investigation of Stardust mission material captured in several impact tracks in silica aerogel collectors (Brownlee et al., 2006; Flynn et al., 2006; Zolensky et al., 2006) has shown that, in contrast to these expectations, a large percentage of the impacted mineral grains are high temperature crystalline grains, such as forsteritic olivine, low Ca pyroxenes (Zolensky et al., 2006), protoenstatite (Schmitz and Brenker, 2008) and Ca, Al-rich inclusions (CAI) (Brownlee et al., 2006; Zolensky et al., 2006). Brownlee et al. (2006), McKeegan et al. (2006) and Zolensky et al. (2006) reported preliminary results about the first CAI-like material, named "Inti", found in Stardust mission impact tracks, which was later studied in greater detail by Simon et al. (2008). The grain "Inti" from Track 25 consists of several refractory minerals – V-bearing osbornite [(Ti,V)N], corundum, probably perovskite, gehlenite, spinel, Ca-, Al-, Ti-rich clinopyroxene, anorthite and FeS (Zolensky et al., 2006; Simon et al., 2008). Simon et al. (2008) used several destructive and non-destructive techniques for determining the mineralogy, chemistry and isotopic composition of the grain. They reported striking similarities in mineralogy, chemistry, Ti oxidation state and oxygen isotopic composition between "Inti" and common CAIs that are found in carbonaceous chondrites and are consistent with condensation from a cooling gas of solar composition.

CAIs are believed to have formed in the solar nebula by condensation or high temperature processing of pre-condensed material, including evaporation, re-condensation and melting (Amelin et al., 2002 and references within) and are the oldest solid objects formed in the solar system (4567.2 ± 0.6 Ma; Amelin et al., 2002). They are typically found in carbonaceous chondrites and are rare in ordinary and enstatite chondrites. CAIs are mineralogically dominated by silicates and oxides that are enriched in Ca and Al, including corundum, hibonite, grossite, perovskite, spinel and anorthite, also melilite and Ti-, Al-diopside (fassaite). Grossman and Clark (1973) concluded that for example titaniferous pyroxenes and melilites found in CAIs indicate an origin via condensation of solar nebula material at temperatures of at least 1400 K. Solar nebula condensates, however, are rare among CAIs, which typically experienced a complex (multistage) history, including episodes of processing within the solar nebula and after accretion within the parent body like induced partial melting and secondary alteration (e.g., MacPherson and Davis, 1993; Beckett et al., 2000; Grossman et al., 2002; MacPherson et al., 2005).

The wide compositional range of crystalline olivine and pyroxenes in Wild 2 suggests that they formed under variable conditions (e.g., oxygen fugacity, temperature) and possibly in different regions of the solar nebula (Zolensky et al., 2006).

Thus, the presence of CAIs and other high temperature phases in Wild 2 indicate that large-scale transport of rocky material must have occurred from the hot inner region of the solar nebula to the cold outer parts (~30 AU) where Kuiper Belt comets formed (Brownlee et al., 2006; McKeegan et al., 2006; Zolensky et al., 2006).

Here we present the detection of additional CAI-like material found in the impact track 110 [C2012, 0, 110, 0, 0] a non-destructive technique. In the past, mineral identification has been made mainly by extracting particles, slicing them up and performing TEM (transmission electron microscopy) analysis which is a time-consuming and complex process. SR-XRF however, being a non-destructive method, does not require special preparation of the impact tracks and allows the analysis of crystalline grains without extraction from the aerogel.

The analyzed impact track reveals at least 2 fragments that are enriched in Ca and Ti. Since CAIs are defined as being Ca-, Al-rich inclusions, it is a major drawback of the SR-XRF detection in ambient conditions that Al cannot be measured. The chemical composition was quantified applying the Fundamental Parameter Method (FPM) and principle component analysis (PCA, Pearson, 1901). Results yield that the grain compositions in the studied regions are close to anorthite ($CaAl_2Si_2O_8$) or grossite ($CaAl_4O_7$) and gehlenite ($Ca_2Al_2SiO_7$), monticellite ($CaMgSiO_4$) or Dmitryivanovite ($CaAl_2O_4$), respectively. Our results are in agreement with observations of the first Stardust CAI "Inti".

2. EXPERIMENTAL

2.1. Sample description

The impact track studied was received inside a keystone which is a piece of dissected aerogel. The preparation was following the technique described in Westphal et al. (2004) at the Space Science Laboratory at University of California at Berkley. For the cutting procedure microneedles were used for extracting the whole impact track out of the collector. Typically, 10 μm of aerogel between the wall of the impact track and the vertical cut is left. Keystones were fragile and therefore fixed on self-supporting "microforklifts" and mounted on a 1 mm-diameter glass needle.

The keystone analyzed in this study was extracted from cell C2012 and contained a carrot shaped impact track (Track 110) with an end particle (terminal particle, TP) and several fragments along the wall of the track. The im-

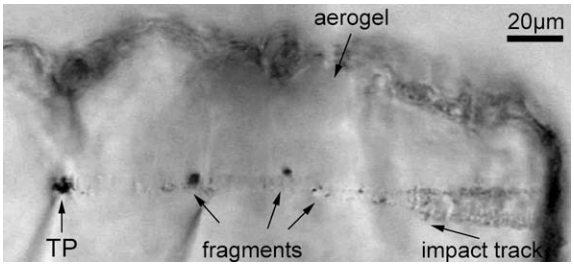

Fig. 1. Stardust impact track 110 [C2012, 0, 100, 0, 0] with a total length of approx. 180 μm and a well defined TP at its end and several larger (>1 μm) and smaller fragments along the wall of the track.

pact track has a total length of approximately 180 μm (Fig. 1).

2.2. Synchrotron radiation XRF set-up

The entire impact track 110 was analyzed with synchrotron radiation (SR) induced X-ray fluorescence (XRF) at the European Synchrotron Radiation Facility (ESRF) in Grenoble (France). The set-up was installed at the nano-focussing beamline ID13. SR from second and third generation sources offer the possibility of non-destructive multi-element analysis with high spatial resolution (see also: Schroer et al., 2005) down to trace element concentrations with relative detection limits (DL) at the sub-ppm range and absolute DL below 1 fg.

The ID13 beamline has a 18 mm period in-vacuum undulator X-ray source and is equipped with a liquid N_2 cooled Si(1 1 1) double crystal monochromator. The excitation X-ray energy of 12.7 keV combined with the detection in air allowed the collection of fluorescence radiation of elements between Si and Se. Thus, Al and Mg content cannot be measured and Si was not quantified, in general, due to the silica aerogel interference which is a severe limitation in identifying minerals.

The incident X-ray beam size obtained was $300 \times 1000\ nm^2$ at a flux of 9.7×10^{10} ph/s using two Be-lenses and $300 \times 300\ nm^2$ with one Be-lens at a lower flux of 3.9×10^9 ph/s. The fluorescence radiation was simultaneously collected in a confocal and a conventional detection mode (Fig. 2) with an energy-dispersive Si(Li) detector and a Vortex Si drift detector placed in a 90° geometry to reduce background signals. The simultaneous collection enables us to directly compare the result of both detection modes.

The confocal detection mode (Kanngießer et al., 2003; Vincze et al., 2004; Brenker et al., 2005; Malzer, 2006) was realized with a polycapillary half lens which was positioned in the detection channel of a Vortex detector. The probing volume depends on the acceptance of the polycapillary and is defined as the intersection of the focus of the half lens with the incident nano X-ray beam. The working distance of the half lens was only a few mm (<10 mm) and the acceptance full width at half maximum (FWHM) in the direction perpendicular to the capillary was determined to be approximately 19 μm for Fe-Kα. A clear advantage of this confocal detection mode is that it strongly reduces the fluorescence signal produced by the aerogel and its contaminants.

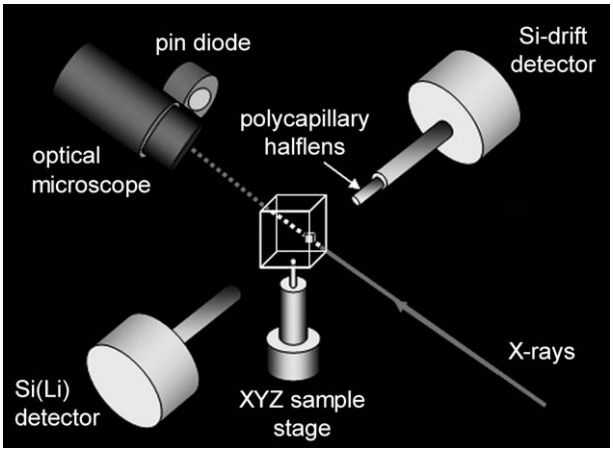

Fig. 2. Sketch of the experimental set-up used at beamline ID13: detection of the fluorescence radiation in a conventional (left) and confocal (right) detection mode. The polycapillary in front of the Si-drift detector defines the probing volume (indicated as a box) of the sample (in confocal detection mode).

The sample, an aerogel "keystone" containing an impact track with comet dust embedded along it, is mounted on a glass–fiber on top of a so called nano cube to allow step precision at the nm-scale. The keystone was moved through the incident nano X-ray beam to perform large "overview" XRF mappings along the impact track, detailed single grain mappings and point analyses. Point measurements (300 s) and scans over smaller areas (e.g., $3 \times 3\ \mu m^2$ up to $6 \times 6\ \mu m^2$) were performed simultaneously in confocal and conventional detection mode in order to compare signals that derived from the particle regions which contain only little contribution of the aerogel ("real signal") and signals which include considerably more of the surrounding aerogel due to the excitation of the aerogel in the beam path before and after the particle.

2.3. Data evaluation

The first step of spectral evaluation was performed using the AXIL software package (Vekemans et al., 1995) for elemental identification and the determination of the net-line intensities. The latter includes background subtraction and the separation of overlapping fluorescence lines. The elemental maps were created using the software package MICROXRF2 (Vekemans et al., 1995) and PyMCA (Solé et al., 2007).

The point measurements obtained in the confocal detection mode were quantified using a model based on the Fundamental Parameter Method (FPM; see Sherman, 1955), which was modified to include the specific properties of the confocal set-up (transmission, energy-dependent acceptance). The net-line intensity ($I_{i,K\alpha}$) of an element can be described by the following equation:

$$I_{i,K\alpha} = I_0 G w_i Q_{i,K\alpha} \tau_{i,K\alpha} \epsilon_{i,K\alpha} \Pi_{exc} \Pi_{fluo} \rho T^{acc}_{i,K\alpha} A_{corr,i,T^{acc}}$$

with:

$I_{i,K\alpha}$ = the Kα net line intensity of element i

I_0 = the intensity of the incoming beam

G = geometry factor

w_i = the weight fraction of element i in the layer of interest

$Q_{i,K\alpha}$ = the XRF production cross section (cm^2/g) of Kα photons for element i

$\tau_{i,K\alpha}$ = polycapillary transmission coefficient for Kα photons of element i

$\varepsilon_{i,K\alpha}$ = detector efficiency for Kα photons of element i

Π_{exc} and Π_{fluo} = terms correcting for the absorption of the incoming beam and fluorescence respectively, by the sample and the surrounding air

ρ = the density of the layer of interest

$T_{i,K\alpha}{}^{acc}$ = the acceptance (FWHM) of the polycapillary for Kα photons of element i

$A_{corr,i,Tacc}$ = absorption correction term for the fraction of the layer of interest that lies within the detector acceptance

This equation was constructed for measurements on both the sample (u) and a standard (s), after which the ratio of both was observed:

$$\frac{I^{(u)}_{i,\mathrm{K}\alpha}}{I^{(s)}_{i,\mathrm{K}\alpha}} = \frac{I^{(u)}_0 G w^{(u)}_i Q_{i,\mathrm{K}\alpha}\tau_{i,\mathrm{K}\alpha}\epsilon_{i,\mathrm{K}\alpha}\Pi^{(u)}_{exc}\Pi^{(u)}_{fluo}\rho^{(u)}T^{acc}_{i,\mathrm{K}\alpha}A^{(u)}_{corr,i,T^{acc}}}{I^{(s)}_0 G w^{(s)}_i Q_{i,\mathrm{K}\alpha}\tau_{i,\mathrm{K}\alpha}\epsilon_{i,\mathrm{K}\alpha}\Pi^{(s)}_{exc}\Pi^{(s)}_{fluo}\rho^{(s)}T^{acc}_{i,\mathrm{K}\alpha}A^{(s)}_{corr,i,T^{acc}}}$$

Several terms can be cancelled out in the numerator and denominator, yielding:

$$\frac{I^{(u)}_{i\mathrm{K}\alpha}}{I^{(s)}_{i\mathrm{K}\alpha}} = \frac{I^{(u)}_0 w^{(u)}_i \Pi^{(u)}_{exc}\Pi^{(u)}_{fluo}\rho^{(u)}A^{(u)}_{corr,i,T^{acc}}}{I^{(s)}_0 w^{(s)}_i \Pi^{(s)}_{exc}\Pi^{(s)}_{fluo}\rho^{(s)}A^{(u)}_{corr,i,T^{acc}}}$$

The system of equations was then solved in an iterative manner for all elements i, using software developed at the XMI group (Gent University, Belgium), yielding the weight fractions $w_i^{(u)}$.

A 93 μm thick geological glass standard ATHO-G (Jochum et al., 2000) with certified elemental concentrations was used as the standard reference material for the FPM quantification. The differences in thickness and composition of the sample and standard have been taken into account using the absorption correction terms $A_{corr,i,Tacc}$ and the Π_{exc} and Π_{fluo} terms that correct for absorption in the sample and the surrounding air. A line scan of 11 points was performed with 30 s measurement time per point, and the resulting normalized sum spectrum was used to determine the elemental yields that are applied to the normalized point spectra obtained from the Stardust grains.

Principle component analysis (PCA; Pearson, 1901) was performed on the elemental concentrations (Ca, Ti, Fe, Ni) obtained from the point spectra and compared to well known Ca and Ti enriched mineral phases and minerals formed in the condensation sequence. PCA is a technique used to reduce multidimensional data sets to lower dimensions for analysis by retaining the orthogonal linear combinations of the original variables (principle components) in the data set that contribute the most to the total variance in the data set. It is mathematically defined as an orthogonal linear transformation of the data to a new coordinate system. Any projection of the data set on the first coordinate has the greatest variance (first principal component, PC1), the second largest variance on the second coordinate (PC2), and so on. PCA is a useful statistical tool to reduce the dimensionality of the data and therefore to summarize the most important parts while simultaneously filtering out noise. The description of the specific PCA method used is given elsewhere (Vekemans et al., 1997).

3. RESULTS

The broad overview map (Fig. 3, step size = 1 μm, RT = 0.5 s, scanned area: 180 × 20 μm^2) of impact track 110 yields a terminal particle and at least four sub-particles along the track which have been characterized and localized by their Ca, Ti, Fe, Ni and Mn content. We identified two Fe, Ni-rich fragments and a single Ti-rich particle, but the most interesting observation are two Ca, Ti-rich grains (the TP and a particle along the track) at the end of the impact track, which also show some local enrichment in Fe and Ni.

Fig. 3. 2D XRF maps of the entire impact track 110 [C2012, 0, 100, 0, 0] for the elements Ca, Ti, Fe and Ni (all Kα-lines). The terminal particle Arthur (far left) is characterized by elevated Ca, Ti, Fe and Ni concentrations. The grain Marvin can be recognized by elevated Ca, Ti and Fe signals. Along the track there are some more fragments enriched in Fe and Ni. One fragment shows only Ti signal. The entrance of the impact track is located at the far right.

3.1. Comparison between confocal and conventional detection mode

Previous SR-XRF measurements on Stardust impact tracks (e.g., Flynn et al., 2006; Ishii et al., 2008; Lanzirotti et al., 2008), which relied on conventional detection modes, have suffered from aerogel contamination in the fluorescence signal. The use of confocal detection allows the suppression of the fluorescence signal from the aerogel which can be demonstrated in Fig. 4. Fig. 4 shows the comparison of both conventional and confocal detection modes using the Pt-Lα line as an example. In the "conventional" (upper) map, several Pt-Lα hotspots are displayed in the 6 × 6 μm^2 sized map representing fluorescence signal that is not produced in the grain itself. The "confocal" (lower) map shows that the signal of the Pt-Lα can be efficiently suppressed with the smaller probing volume, demonstrating the collimating effect of the polycapillary.

The corresponding sum spectra for the related scanned area also illustrate the suppression of the surrounding aerogel which becomes obvious especially for the Se-Kα line but also for As-Kα and Pt-Lα lines. The distribution of Se around the particle representing compressed aerogel was recently demonstrated by Silversmit et al. (2009). The use of confocal detection mode therefore offers the advantage of detecting fluorescence almost exclusively from the region of interest (here: the particles). It is known that compacted or molten aerogel around the grains lead to a relative increase in concentrations of elements present in the aerogel (Tsou et al., 2003).

3.2. FPM: concentrations obtained on CAI-like material

A severe limitation on identifying mineral phases using XRF techniques is the strong absorption of Al, Mg and O fluorescence radiation that makes it impossible to detect these elements with the used set-up. Furthermore, the Si content cannot be measured quantitatively due to interference of the aerogel. Therefore, the interpretation of the data

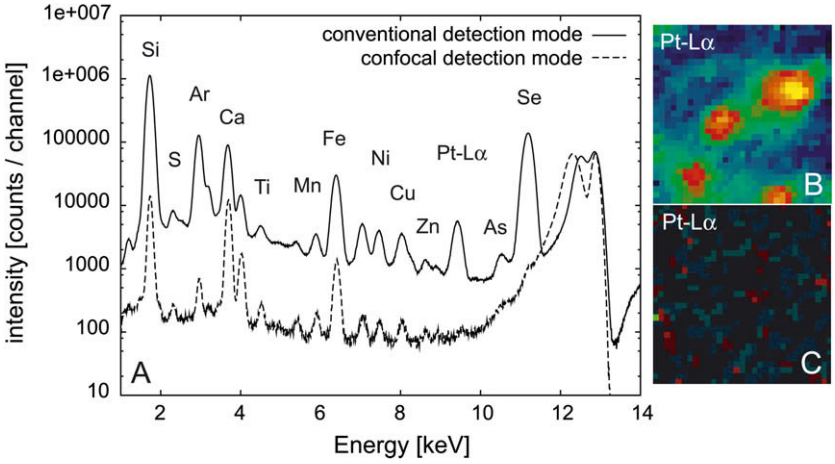

Fig. 4. (A) The comparison between the confocal and conventional detection mode shown for the two sum spectra demonstrating the efficient suppression of signal from the surrounding aerogel (e.g., Se, As, Pt). The 2D XRF maps for the element Pt-Lα in the conventional (B) and confocal (C) detection mode also show the advantage of the confocal mode by efficient suppression of the signal from the aerogel (size of XRF maps is 6×6 μm^2).

is mainly based on the Ca and Ti content revealing CAI-like candidates. The detailed XRF analysis confirms the two hotspots enriched in Ca and Ti.

The approximately 2×2 μm^2 sized terminal particle (TP, "Arthur"[1]) and a second 1.5×1.5 μm^2 sized fragment (hereafter: "Marvin") reveal Ca concentrations of a few wt.% together with a slight enrichment in Ti.

The two-dimensional (2D) XRF maps obtained with the confocal mode are shown in Fig. 5(A,B). The figures show that the higher concentrations of the elements Ca, Ti, Fe and Ni do not coincide, but overlap. This can be demonstrated in a RGB plot (Fig. 5C,D) which clearly shows the different positions for the elemental maxima. For the TP Arthur, the highest concentrations of Ca and Ti have different positions, whereas the Ca, Fe and Ni contents seem to correlate. For the grain Marvin it can clearly been seen that the highest concentrations of all three elements Fe, Ti and Ca have different positions in the map and only the lower concentrations of each element slightly overlap.

First order results from the FPM quantification of seven point spectra (s66–s68, s73, s186, s191, s196) obtained in the confocal detection mode from the two Ca-rich particles (Marvin and Arthur) are listed in Table 1. Fig. 6 shows three representative spectra of Arthur (s73) and Marvin (s186, s196) for confocal and conventional detection mode. For the FPM quantification, parameters like the particle size, particle density and matrix have to be defined.

The particle size can easily be estimated using the 2D XRF maps and measuring the mean diameter of the particles. A size of 2.0 μm for Arthur and 1.5 μm for Marvin was used for the quantification model. One crucial step was the approximation of the density of each particle. For the final quantification, a mean density of 3.5 g/cm^3 was assumed. A variation of density values between 3.0 g/cm^3 and 4.0 g/cm^3 was applied in order to estimate the maximum error introduced for the FPM. The starting matrix was set to SiO_2 because CAIs are comprised primarily of silicate minerals. Variation of the starting matrix of the model leads to much smaller changes than varying the density and is therefore considered only as second order effect (see Table 2). The variation of the starting matrix, e.g., Al_2O_3 instead of SiO_2, leads to deviations in the quantification of less than 1%. The total error for the quantification method was estimated to be up to 16%, dominated by the density of the particle.

The results from the terminal particle Arthur (Table 1) show that, except for one point measurement, all spectra (s66–s68) yield low concentrations of the measured elements, most likely representing a SiO_2 (aerogel) matrix with only minor enrichment of different elements. This might be due to low count rates. An explanation could be that these measurements were performed at the surface of the fragments leading to a low amount of fluorescence radiation. Only one point, measured under optimized conditions (s73, Fig. 6A), shows a Ca, Ti, Fe and Ni enrichment. This measurement was performed at the "hot spot", the region of highest count rate, reflecting that the fluorescence radiation came from the total volume of the particle at this point. The Ca concentration was calculated to 27 wt.% (Ti = 0.1, Fe = 2.58, Ni = 0.12, Mn = 0.14 wt.%) (Table 1). For PCA, only this measurement was considered as representative for the TP.

The measurements of grain Marvin gave much better results due to higher counts in the confocal mode. Measurement s186 represents a point spectrum from the Fe-rich part of the phase (Fig. 6B); s191 was taken at the maximum Ti concentration and s196 at the Ca maximum (Fig. 6C). The Ca concentrations for s191 and s196 vary between 13 and 13.5 wt.%, Ti and Fe are approx. 1 wt.%. In comparison to Arthur, the Ni concentration is only 52 ppm at s196 and 140 ppm at s191. The point measurement s186 shows lower concentrations for all elements: Ca = 0.16, Fe = 1.68, Ti and Ni 0.03 (all in wt.%) possibly representing

[1] Particle names from "The hitchhiker's guide to the galaxy" by Douglas Adams.

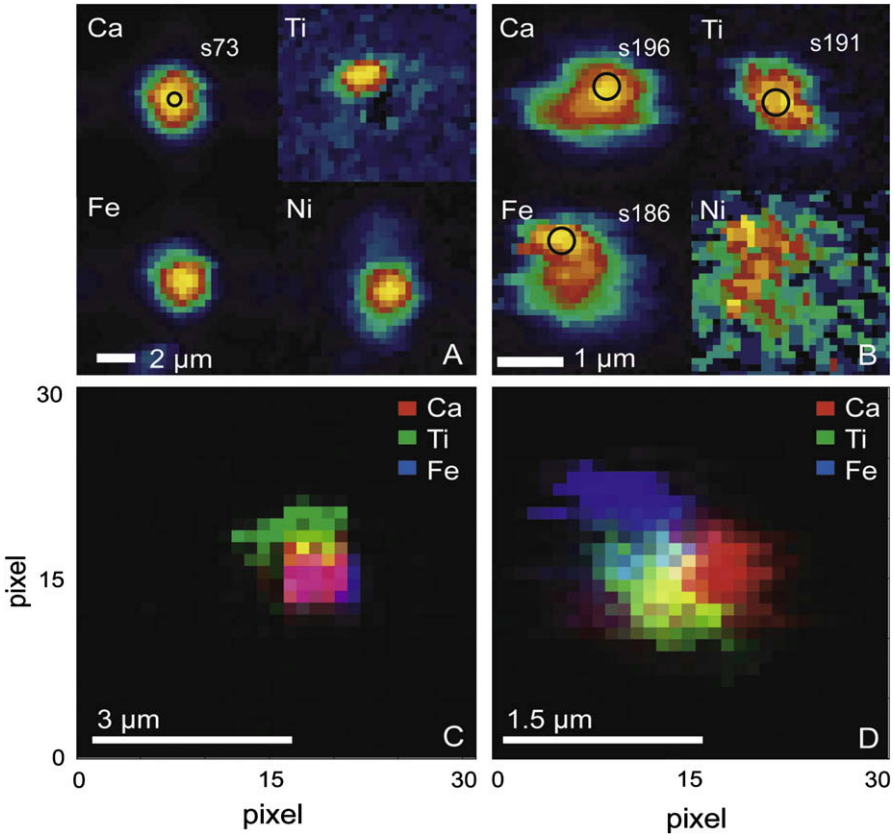

Fig. 5. (Top) Confocal 2D XRF maps for the TP Arthur (A) and for the grain Marvin (B) for the elements Ca, Ti, Fe and Ni. The circles indicate the spot measurement positions (not to scale). (Below) The RGB maps including the elements Ca, Ti and Fe show different hotspots in elemental concentrations related to a polyphase mineral character. Especially for Marvin it is clear that the three elements are uncorrelated.

a different (Mg-, Al and/or Si-rich) mineral phase or another measurement that was performed at the surface of the grain revealing similar problems as for the TP (s66–s68).

The maximum error obtained for the FPM due to variation of the particle size (d), particle density (ρ) and the matrix parameters is listed in Table 2 where the variations are shown with respect to the first column. The estimation of d is the most critical parameter for the quantification model and can result in deviations up to 25%, but fortunately it can be eliminated by measuring the true particle size from the 2D XRF map. Therefore the error of the quantification model is dominated by the variation of the assumed density alone, which is 15% for Ca, Ti and 16–16.5% for the other elements. The variation of the starting matrix (assuming Al-rich phases instead of Si-rich phases) leads to errors which can be neglected with respect to the larger errors discussed above.

Table 1
Concentrations obtained for the terminal particle Arthur and the grain Marvin using FPM (data in wt.% except for asterisks representing data in ppm). Only the data of s73, s186, s191 and s196 are used for PCA. Si and O are included due to the chosen starting matrix.

	Arthur concentrations				Marvin concentrations		
	s66	s67	s68	s73	s186	s191	s196
Ca	0.13	0.23	0.20	27.42	0.17	12.97	13.45
Ti	1*	11*	13*	0.10	0.04	0.87	0.81
Cr	15*	14*	14*	0.02	nd	nd	nd
Mn	13*	2*	16*	0.14	0.05	0.13	0.12
Fe	62*	158*	103*	2.58	1.68	1.00	0.98
Co	nd	nd	nd	nd	85*	32*	57*
Ni	7*	8*	4*	0.12	316*	140*	52*
Si	45.93	45.88	45.90	32.02	45.09	39.10	38.93
O	53.92	53.86	53.88	37.59	52.93	45.90	45.70

nd = not detected.

The similarity of Arthur and Marvin with minerals that are well known from the CAI condensation sequence like hibonite, grossite, perovskite, Dmitryivanovite, gehlenite, spinel, diopside/Ti-, Al-diopside (fassaite) etc. (see Fig. 7) as well as additional mineral phases that are enriched in Ca (e.g., wollastonite, augite) is explored by performing PCA using the elements Ca, Ti, Fe and Ni. Si was avoided due to possible interferences from the aerogel, and Al and Mg cannot be measured with the applied SR-XRF set-up. The elements Mn, Cr, Zn and Co may appear in different reference minerals as trace elements but are not really indicative of the identity of the host minerals.

The components PC1 and PC2 (Fig. 7) show the greatest contribution to the variance in concentrations

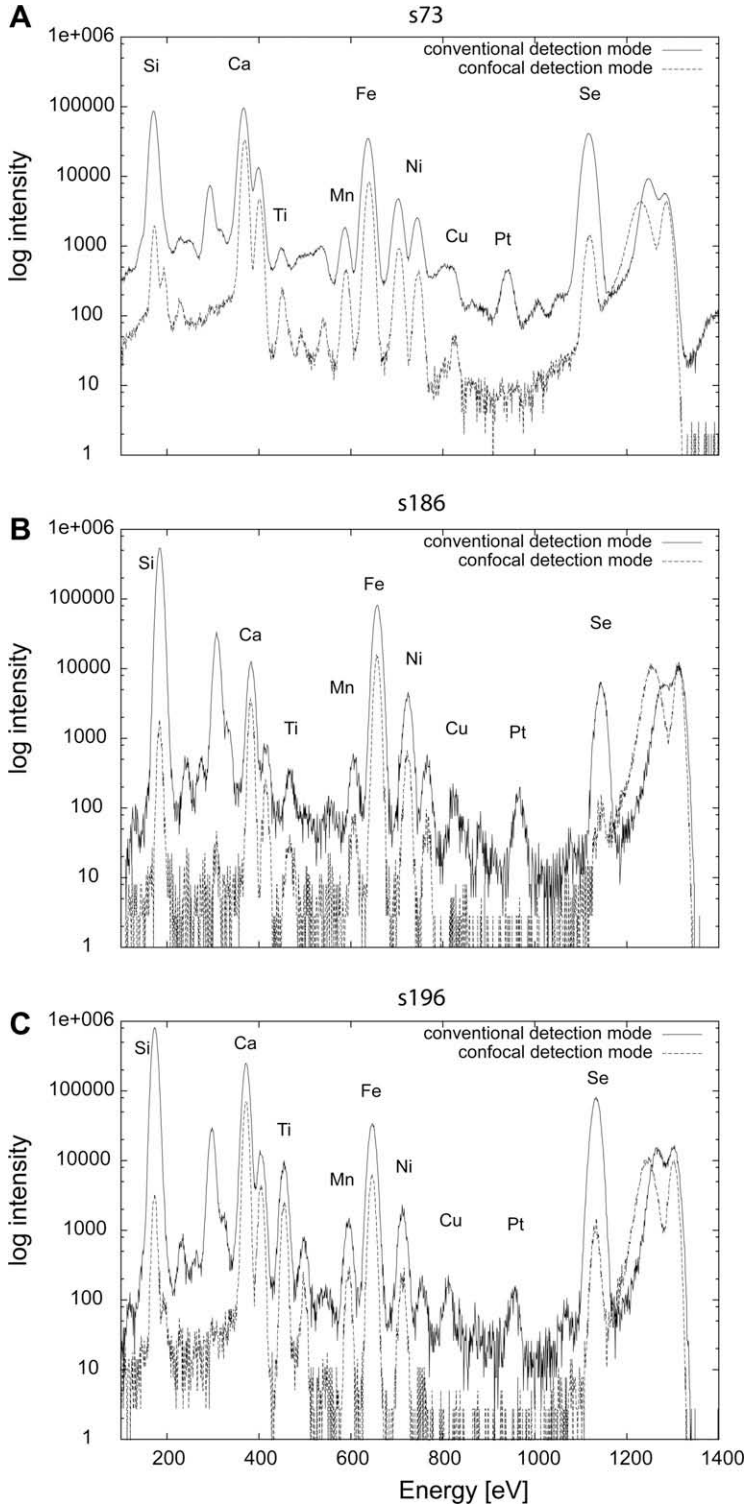

Fig. 6. Point spectra of the Arthur grain (s73) and the Marvin grain (s186, s196) in the conventional and confocal detection mode. Measurements were performed simultaneously in both detection modes for 300 s. The spectra of the confocal mode were used for quantification based on Fundamental Parameter Methods.

(PC1 = 84.32%, PC2 = 10.82%), whereas the third component has only a minor contribution of 4.86%. The PC1 vs. PC2 plot is dominated by Ca (high weight to PC1) and Ti (high weight to PC2). The contribution of Fe and Ni to PC1 and PC2 is negligible as shown in the loading plot (inset of Fig. 7), indicating that the variance in the concentra-

Table 2
Maximum error for the FPM obtained on data from the Arthur grain. Error is based on the variation of the parameters d, ρ and the matrix. Errors are shown with respect to the first (initial) column. The variation of d represents the most critical step for the quantification model but can be eliminated by measuring the particle size in the 2D maps. Therefore, the error is dominated by the variation of the assumed density and is 15% for Ca, Ti and 16–16.5% for the other elements.

Element	Initial	Varying d		Varying ρ				Varying matrix	
	wt.%	wt.%	Δ	wt.%	Δ	wt.%	Δ	wt.%	Δ
Ca	35.72	27.43	8.29	41.26	5.54	31.57	4.15	35.58	0.14
Ti	0.14	0.10	0.04	0.16	0.02	0.12	0.02	0.13	0.01
Cr	0.03	0.02	0.01	0.03	0.00	0.02	0.01	0.03	0.00
Mn	0.18	0.14	0.04	0.21	0.03	0.16	0.02	0.18	0.00
Fe	3.41	2.58	0.83	3.97	0.56	2.99	0.42	3.41	0.00
Ni	0.16	0.12	0.04	0.19	0.03	0.14	0.02	0.16	0.00
d (μm)	1.5	2.0		1.5		1.5		1.5	
ρ (g/cm^3)	3.5	3.5		3.0		4.0		3.5	

tion data can be explained mainly by the concentration variations in Ca and Ti. The classification of Arthur and Marvin as seen in Fig. 7 can then be easily understood in the following way.

A Ca-trend line extends from point 6 (spinel) to point 16 (larnite) and separates the plot into fields of Ti-free and Ti-bearing mineral phases. Minerals on the Ca-trend line are Ti-free; each mineral which plots above contains Ti. Although hedenbergite does not contain Ti it is shifted below the line due to the higher Fe-content. A high Ti content (upper half of the plot) would correspond to titanite or perovskite; a high Ca value corresponds to Ca-rich phases, e.g., gehlenite, rankinite or larnite. The inset of Fig. 7 (loading plot) shows Fe and Ni in the left edge of the lower half in the plot close to the origin of the coordinate system. As mentioned before, Fe and Ni do not contribute much to the PC1 vs. PC2 plot due to a small variation in the data set. Also, minerals containing little to no Ca and Ti should show up close to the origin of the plot (e.g., spinel). It is interesting to see that the grouping of these minerals is possible on the basis of Ca and Ti.

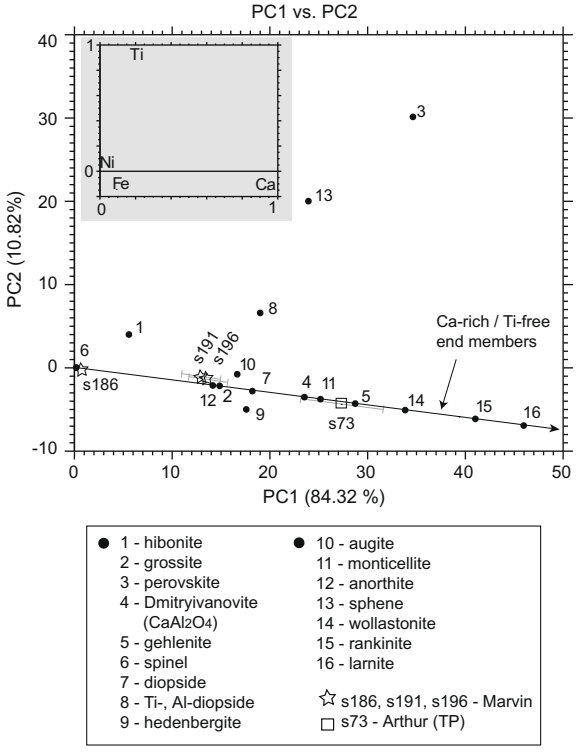

Fig. 7. The PC1 vs. PC2 discrimination diagram for the elements Ca, Ti, Fe and Ni shows Ca-rich minerals and minerals from the condensation sequence in comparison to the Ca, Ti enriched grains from track 110. The plot is dominated by Ca and Ti, whereas Fe and Ni do not contribute much which can be also seen in the inset of the plot (loading plot). The Ca, Ti composition of the terminal particle Arthur is consistent to the composition of gehlenite, monticellite and Dmitryivanovite ($CaAl_2O_4$). The measured positions of the grain Marvin (except for one point) are consistent with anorthite or grossite.

The classification of the TP Arthur is limited to a single measurement that has sufficient counts. Square s73 represents the maximum intensity obtained from the TP and within error (represented by the arrows) it plots close to points 4, 5 and 11. This means, that the Ca and Ti concentrations of the point s73 is similar to the Ca and Ti concentration of gehlenite, monticellite or Dmitryivanovite that lies at the maximum end of the error region. Table 3 shows a direct comparison of the Ca, Ti and Fe concentrations of these three minerals and Arthur. From comparison of the Ca content Arthur is more consistent with gehlenite and monticellite than with Dmitryivanovite. The stars s186, s191 and s196 represent the grain Marvin. The stars s191 and s196 are close to the points 2 and 12 – grossite and

Table 3
Direct comparison of the Ca, Ti and Fe content of the Arthur and Marvin grain with the "standard" minerals that fit best. All data are given in wt.%.

Element	s73	Monticellite	Gehlenite	Dmitryivanovite
Ca	27.42	25.61	29.23	23.94
Ti	0.10	0.00	0.00	0.00
Fe	2.58	0.00	0.00	0.00
Element	**s191**	**s196**	**Anorthite**	**Grossite**
Ca	12.97	13.45	14.4	15.08
Ti	0.87	0.81	0.00	0.09
Fe	1.00	0.98	0.00	0.24

anorthite. From the direct comparison of the Ca, Ti and Fe content (Table 3) s191 and s196 are slightly more consistent with the Ca content of anorthite than grossite although the Ti and Fe concentrations are higher than the "standard" minerals. Star s186 is close to the origin of the coordinate system which indicates lower Ca, Ti concentration compared to the two other points which is in agreement to Table 1.

4. DISCUSSION AND CONCLUSIONS

Our work demonstrates the high potential of SR-XRF to identify CAI-like fragments in Stardust impact tracks without any complex, time-consuming, destructive sample preparation. The non-destructive in situ (impact track covered with aerogel) technique protects the samples from any contamination and allows the pre-selection of interesting tracks for specific scientific questions. Before extracting and preparing the grains, it is thus a good opportunity for quantitative multi-elemental analyses down to the trace element level. The keystone can be used afterwards for other methods which need special preparation (e.g., TEM) and are (in most of the cases) destructive on at least at the nm-scale (e.g., NanoSIMS, TOF-SIMS).

A high spatial resolution of some hundred nm (in best cases less than 50 nm (Schroer et al., 2005)) can be obtained with still sufficiently high photon flux on the ID13 beamline at the ERSF. It is further demonstrated that by using a confocal set-up, it is possible to minimize the amount of fluorescence signal from the surrounding aerogel matrix. Due to the unequal distribution of impurities and compression of the aerogel, the confocal mode provides the possibility of extracting almost only the fluorescence radiation of the grain itself.

Our SR-XRF results show that there are two CAI-like fragments present in the impact track 110. Ca concentrations of 13 and 27 wt.% are obtained in the Ca-rich regions of the particles.

Applying PCA to discriminate the mineral phases suggests that one fragment (TP) mainly is consistent with gehlenite, monticellite or Dmitryivanovite, whereas the second particle is consistent with primarily anorthite or grossite. Due to the high spatial resolution offered by the set-up, it is possible to show that the fragments consist of several chemically diverse mineral phases. The RGB maps (Fig. 5C,D) illustrate that the highest concentrations for the elements do not correlate. The polyphase nature of the fragments is in agreement with the results from the Stardust CAI "Inti" which also shows a complex chemical structure due to a mixture of several different mineral phases.

At the entrance region of the impact track we detected a Ti-rich fragment. It is less than several 100 nm in size which makes the quantification more difficult. Within the XRF spectrum only a very low Ca signal (only a few 100 counts) with respect to the other measurements of Marvin or Arthur is found. During penetration and deceleration of the original impacting particle through the aerogel, the incident particle often breaks into several pieces and thus the Ti phase at the entrance region of the track might be originally part of the CAI-like fragments. In this case, likely candidates for the grain are Ti-oxide (TiO_2) or TiN. Osbornite [(Ti,V)N] was also reported by Zolensky et al. (2006) and Simon et al. (2008), as part of the Ca-, Al-rich inclusion "Inti".

A major drawback of the SR-XRF technique is the problem that Al and Mg cannot be measured due to the strong absorption of the fluorescence radiation by the aerogel matrix and the ambient measuring conditions and that Si cannot be quantitatively measured due to interference of the aerogel. Since CAIs are comprised of primarily silicate minerals only Ca and Ti can be used as indicators for CAI-like candidates. Nevertheless, this technique is a first (non-destructive and easy) way in identifying those candidates still in the aerogel. Afterwards, other techniques that are more time-consuming and complex in sample preparation (e.g., for TEM, NanoSIMS analysis) can be applied to those particles. The second step is needed to confirm the SR-XRF data.

The presence of additional CAI-like materials in comet 81P/Wild 2 samples strengthens the hypothesis that comets are not formed in isolation in the cold icy region of the solar system. Highly refractory minerals found in cold icy and dusty objects, require a large-scale radial mixing in the protoplanetary disk with a mass transport from the inner part of the solar nebula to its outer parts. Gehlenite for example would condense from a cooling gas of solar composition at temperatures of >1600 K; anorthite at a slightly lower temperature of 1416 K. Due to their formation temperature of 1400–2000 K, CAIs are believed to originate from very close to the proto-Sun. Mixing processes must occur over distances to at least 30 AU (A'Hearn, 2006) where short period comets were formed in the Kuiper belt and refractory minerals were implanted.

ACKNOWLEDGEMENTS

This work was funded by the Deutsche Forschungsgemeinschaft (DFG BR2015/11). This research was also performed as part of the "Interuniversity Attraction Poles" (IAP6) Programme financed by the Belgian government. Dr. G. Silversmit is supported by a postdoctoral fellowship from the Research Foundation-Flanders (FWO-Vlaanderen, Belgium). We thank Gerald Falkenberg (DESY, HASYLAB, Germany) for providing the polycapillary halflens for the SR-XRF measurements. We also thank the Stardust PET and the JSC curation facility for preparing and providing the sample. We are grateful to Hope Ishii, Mike Zolensky, one anonymous reviewer and the Associate Editor Sasha Krot for their comments which helped much to improve the manuscript.

REFERENCES

A'Hearn M. F. A. (2006) Whence Comets? *Science* **314**, 1708–1709.

Amelin Y., Krot A. N., Hutcheon I. D. and Ulyanov A. A. (2002) Lead isotopic ages of chondrules and calcium–aluminium-rich inclusions. *Science* **297**, 1678–1683.

Beckett J. R., Simon S. B. and Stolper E. (2000) The partitioning of Na between melilite and liquid: part II. Applications to Type B inclusions from carbonaceous chondrites. *Geochim. Cosmochim. Acta* **64**, 2519–2534.

Brenker F. E., Vincze L., Vekemans B., Nasdala L., Stachel T., Vollmer C., Kersten M., Somogyi A., Adams F., Joswig W. and Harris J. W. (2005) Detection of a Ca-rich lithology in the Earth's deep (>300 km) convecting mantle. *Earth Planet. Sci. Lett.* **236**, 579–587.

Brownlee D. et al. (2006) Comet 81P/Wild 2 under a microscope. *Science* **314**, 1711–1716.

Flynn G. J. et al. (2006) Elemental compositions of comet 81P/Wild 2 samples collected by Stardust. *Science* **314**, 1731–1735.

Grossman L. and Clark, Jr., S. P. (1973) High-temperature condensates in chondrites and environment in which they formed. *Geochim. Cosmochim. Acta* **37**, 635–649.

Grossman L., Ebel D. and Simon S. B. (2002) Formation of refractory inclusions by evaporation of condensate precursors. *Geochim. Cosmochim. Acta* **66**, 145–161.

Ishii H., Brennan S., Bradley J. P., Luening K., Ignatyev K. and Pianetta P. (2008) Recovering the elemental composition of comet Wild 2 dust in five Stardust impact tracks and terminal particles in aerogel. *Meteoritics & Planet. Sci.* **43**, 215–231.

Jochum K. P. et al. (2000) The preparation and preliminary characterization of eight geological MPI-DING reference glasses for in situ microanalysis. *Geostandard Newslett.* **24**, 87–133.

Kanngießer B., Malzer W. and Reiche I. (2003) A new 3D micro X-ray fluorescence analysis set-up – first archaeometric applications. *NIB Phys. Res. B* **211**, 259–264.

Lanzirotti A., Sutton S. R., Flynn G., Newville A. and Rao W. (2008) Chemical composition and heterogeneity of Wild 2 cometary particles determined by synchrotron X-ray. *Meteoritics & Planet. Sci.* **43**, 187–213.

Malzer W. (2006) 3D micro X-ray fluorescence analysis. *Rigaku J.* **23**, 40–47.

MacPherson G. J. and Davis A. M. (1993) A petrologic and ion microprobe study of a Vigarano Type B refractory inclusion: evolution by multiple stages of alteration and melting. *Geochim. Cosmochim. Acta* **57**, 231–243.

MacPherson G. J., Simon S. B., Davis A. M., Grossman L. and Krot A. N. (2005) Calcium–aluminium-rich inclusions: major unanswered questions. In *Chondrites and the Protoplanetary Disk*. *ASP Conference Series*, vol. 341 (eds. A. N. Krot, E. R. D. Scott and B. Reipurth). Astronomical Society of the Pacific, San Francisco, pp. 225–251.

McKeegan K. D. et al. (2006) Isotopic composition of cometary matter returned by Stardust. *Science* **314**, 1724–1728.

Pearson K. (1901) On lines and planes of closest fit to systems of points in space. *Philoso. Mag.* **2**, 559–572.

Rotundi A., Baratta G. A., Borg J., Brucato J. R., Busemann H., Colangeli L., D'Hendecourt L., Djouadi Z., Ferrini G., Franchi I. A., Fries M., Grossemy F., Keller L. P., Mennella V., Nakamura K., Nittler L. R., Palumbo M. E., Sandford S. A., Steele A. and Wopenka B. (2008) Combined micro-Raman, micro-infrared, and field emission scanning electron microscope analyses of comet 81P/Wild 2 particles collected by Stardust. *Meteoritics & Planet. Sci.* **43**, 367–397.

Sandford S. A. et al. (2006) Organics captured from comet 81P/Wild 2 by the stardust spacecraft. *Science* **314**, 1720–1724.

Schmitz S. and Brenker F. E. (2008) Microstructural indications for protoenstatite precursor of cometary $MgSiO_3$ pyroxene: a further high-temperature component of Comet Wild2. *Astroph. J. Lett.* **681**, L105–L108.

Schroer C. G., Kurapova O., Patommel J., Boye P., Feldkamp J., Lengeler B., Burghammer M., Riekel C., Vincze L., van der Hart A. and Küchler M. (2005) Hard X-ray nanoprobe based on refractive X-ray lenses. *Appl. Phys. Lett.* **87**, 124103-1–124103-3.

Sherman J. (1955) The theoretical derivation of fluorescence X-ray intensities from mixtures. *Spectrochim. Acta* **7**, 283–306.

Silversmit G., Vekemans B., Brenker F. E., Schmitz S., Burghammer M., Riekel C. and Vincze L. (2009) X-ray fluorescence nanotomography on cometary matter from Comet 81P/Wild2 returned by Stardust. *Anal. Chem.*, in press. doi:10.1021/ac900507x.

Simon S. B., Joswiak D. J., Ishii H. A., Bradley J. P., Chi M., Grossman L., Aléon J., Brownlee D. E., Fallon S., Hutcheon I. D., Matrajt G. and McKeegan K. D. (2008) A Refractory Inclusion Returned by Stardust from Comet P81/Wild 2. *Meteoritics & Planet. Sci.* **43**, 1861–1877.

Solé V. A., Papillon E., Cotte M., Walter P. and Susini J. (2007) A multiplatform code for the analysis of energy-dispersive X-ray fluorescence spectra. *Spectrochim. Acta B* **62**, 63–68.

Tsou P., Brownlee D. E., Hörz F., Sandford S. A. and Zolensky M. E. (2003) Wild 2 and interstellar sample collection and Earth return. *J. Geophys. Res.* **108**(E10), 8113. doi:10.1029/2003JE002109.

Vekemans B., Janssens K., Vincze L., Adams F. and Van Espen P. (1995) Comparison of several background compensation methods useful for evaluation of energy-dispersive X-ray-fluorescence. *Spectrochim. Acta B* **50**, 149–169.

Vekemans B., Janssens K., Vincze L., Aerts A., Adams F. and Hertogen J. (1997) Automated segmentation of mu-XRF image sets. *X-ray Spectrom.* **26**, 333–346.

Vincze L., Vekemans B., Brenker F. E., Falkenberg G., Rickers K., Somogyi A., Kersten M. and Adams F. (2004) Three-dimensional trace element analysis by confocal X-ray microfluorescence imaging. *Anal. Chem.* **76**, 6786–6791.

Westphal A. J., Snead C., Butterworth A., Graham G. A., Bradley J. P., Bajt S., Grant P. G., Bench G., Brennan S. and Pianetta P. (2004) Aerogel keystones: extraction of complete hypervelocity impact events from aerogel collectors. *Meteoritics & Planet. Sci.* **39**, 1375–1386.

Zolensky M. E. et al. (2006) Mineralogy and petrology of comet 81P/Wild 2 nucleus samples. *Science* **314**, 1735–1739.

Associate editor: Alexander N. Krot